GEOPHYSICS, VOL. 73, NO. 5 (SEPTEMBER-OCTOBER 2008); P. VE223–VE233, 20 FIGS.
10.1190/1.2951469

Assessing estimated velocity-depth models: Finding error bars in tomographic inversion

D. A. Chițu[1], M. N. Al-Ali[2], and D. J. Verschuur[1]

ABSTRACT

In conventional migration velocity analysis methods, a velocity model is estimated that results in flattened events in common-image gathers. However, after this process, no information is available on the accuracy of this velocity model. A statistical analysis of velocity-model parameters is very difficult because of the integrated nature of the process. In common-focus-point technology, velocity estimation is split into two processes: a first step to estimate one-way focusing operators from the seismic data and a second step to translate these one-way propagation operators into a velocity-depth model. Because the second step does not involve seismic data and uses a hands-off model parameterization, a statistical analysis of the inversion result becomes rather straightforward. We developed a methodology for obtaining a suite of possible solutions, from which statistical measures can be extracted. By varying initial settings, the inversion of one-way traveltimes provides a space of solutions. Rather than having a single estimated model, we can obtain an ensemble of models. By performing statistical analysis of this ensemble, the error bars of the estimated velocity model can be retrieved. The procedure was tested for a 2D synthetic and field data set, for which the latter compares favorably to a conventional two-way traveltime tomography approach. The information provided by such an analysis is important because it shows the reliability of the final estimated model and could provide feedback for acquisition geometry design. More or better data might be needed to obtain a model to which a smaller degree of ambiguity is associated.

INTRODUCTION

The estimation of a velocity model is an important step in seismic imaging. Seismic data interpretation is based on this model. Thus, the velocity model influences important conclusions such as size and shape of the reservoir and the expected volume of producible hydrocarbons. In conventional migration-velocity analysis (MVA) (Al-Yahya, 1989; Stork, 1992; Kosloff et al., 1996) the flatness of the events in common-image gathers (CIGs) is the criterion in an integrated-velocity model-estimation process. In each iteration, observed residual moveouts are translated into an update of the velocity model. The parameterization of the velocity model is often user defined, such as a layered one (van der Made, 1988; Hegge, 2000) or cell-based methods (Vesnaver et al., 1995). When CIGs show mostly flat events, the velocity model is considered to be final and the image can be produced.

However, during this updating process, little information is available and is analyzed on the reliability of this model. The model is the result of parameters chosen at each iteration update. Another parameterization could have led to another model that also shows mostly flattened events in CIGs. Thus, the resulting image is only one of a complete ensemble of images that all satisfy the seismic data within a certain tolerance.

Alternatively, two-way traveltime tomography methods use picked seismic events in the two-way data (i.e., shot records) as the input (Bishop et al., 1985; van der Made, 1988). The first disadvantage of this method is that traveltimes need to be picked in the raw seismic data, which in some situations suffer from low signal-to-noise ratio (S/N) and complex interference patterns. Furthermore, two-way traveltime tomography requires the description of reflection paths, which might not be obvious in complicated subsurface structures.

In common-focus point (CFP) technology (Berkhout, 1997a and 1997b; Thorbecke, 1997), the estimation of the velocity-depth model is split into two separate processes. First, one-way focusing operators are estimated from the seismic data. This results in a set of one-way traveltimes originating from reflection points toward the surface locations. Second, these one-way traveltimes are translated into a velocity-depth model via tomography (Cox and Verschuur, 2001). This step resembles the earthquake tomography problem, with each

Manuscript received by the Editor 20 December 2007; revised manuscript received 11 March 2008; published online 1 October 2008.
[1]Delft University of Technology, Department of Applied Physics, Laboratory of Acoustical Imaging and Sound Control, Delft, The Netherlands. E-mail: D.A.Chitu@TUDelft.nl; D.J.Verschurr@TUDelft.nl.
[2]Saudi Aramco, KAUST Research Development Department, Dhahran, Saudi Arabia. E-mail: mustafa.ali.2@aramco.com.

reflection point being a virtual earthquake source. The main advantage of this two-step approach is that decisions on parameterization of the velocity-depth model can be postponed to the second stage, which no longer involves seismic data. Another major advantage is that the second step can be subjected easily to multiple trials, resulting in a statistical analysis of the tomographic inversion result.

In this paper, we discuss the statistical analysis of the tomographic inversion. After a short review of tomographic inversion, we show how to assess the accuracy of the velocity-depth model using a synthetic data example. We then link acquisition parameters of the seismic data and the accuracy of the velocity-depth model. Finally, we demonstrate the complete CFP workflow on a 2D field data set from the Middle East.

OVERVIEW OF TOMOGRAPHIC OPERATOR INVERSION

Within CFP technology, the principle of equal time is used to determine focusing operators (Rietveld, 1995; Berkhout, 1997b; Bolte and Verschuur, 1998). These focusing operators can be seen as the response of a secondary source (a focal point) in the subsurface toward receivers at the surface. Therefore, they can be considered one-way Green's functions of the subsurface. The tomographic inversion takes the estimated one-way traveltimes from focal points toward surface locations and finds a velocity-depth model that satisfies these traveltimes. The estimated model consists of velocity values and locations of focal points.

Figure 1 presents the strategy for focusing operator inversion (Cox and Verschuur, 2001; Cox, 2004). An initial model is introduced in which one-way traveltimes are computed by forward modeling. The difference between these modeled and observed one-way traveltimes becomes the data to be inverted. The optimization refers to minimizing traveltime differences to optimize model parameters. The output is updates of model parameters. These updates are added to initial model parameters, and an updated model is obtained. In this model, one-way traveltimes can be recomputed. This is an iterative process; when the differences between observed and modeled traveltimes are small enough, an accurate model is obtained.

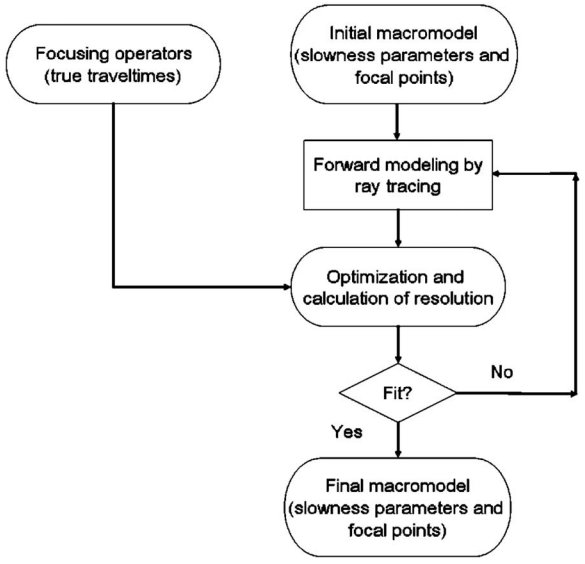

Figure 1. Flowchart describing the tomographic inversion of focusing operators.

The relationship between the one-way traveltime data and model parameters is not linear. We assume this relationship to be linear under the condition of small model-parameter updates. This is represented as

$$\Delta \mathbf{t} = \mathbf{A}\Delta \mathbf{m}. \quad (1)$$

The matrix **A** describes the linear relation and therefore contains derivatives of differences in traveltimes with respect to model-parameter updates. Note that $\Delta \mathbf{t}$ is a vector with differences between the modeled and true one-way traveltimes, and $\Delta \mathbf{m}$ is a vector with desired updates of model parameters.

Estimation of a subsurface model requires parameterization. In two dimensions, this is done with a Delaunay triangulation (Sambridge et al., 1995; Böhm and Vesnaver, 1999). Velocity values are defined at grid points that are totally independent of the focal points. This ensures continuity across interfaces and an optimum number of parameters. The parameterization is modified in a data-driven manner. The density of grid points is higher in regions where more data points are available, compared with regions with less data. The data-driven aspect of this process is given by the fact that these regions are chosen based on resolution values, which are computed along with the inversion (Cox and Verschuur, 2001; Cox, 2004). Thus, no user intervention is required in this process.

Finally, the matrix inversion required to solve equation 1 is done iteratively, using the LSQR algorithm (Paige and Saunders, 1982). This algorithm is a type of conjugate gradient method similar to singular value decomposition (SVD) because it computes approximations of singular values of **A** and corresponding eigenvectors. The algorithm tries to fit the data using a limited number of vectors, so it is a subspace method.

The rank of the inversion **A** enters our approach through a resolution matrix. This matrix indicates the resolved part of the system and the part yet to be solved. The resolution value connected to each parameter tells how well that parameter is determined. Thus, new parameters can be included in regions that are well covered by the data or removed from regions with poor data coverage. In this way, regularization is performed.

STATISTICAL ANALYSIS OF THE ESTIMATED VELOCITY-DEPTH MODEL

The inherent nonuniqueness in the recorded data is a very important factor that deteriorates the accuracy of estimates. Usually, there are features of the true model that cannot be resolved, even if no errors are obtained in one-way traveltimes and the inverse problem is truly linear. This leads to many models fitting the data equally well. The CFP approach is well suited to obtain such an ensemble of models because it involves only the inversion of traveltimes, which have been extracted from the seismic data in a separate process.

Each run of the tomographic inversion with unique initial settings leads us toward a different estimated velocity-depth model. This estimated model explains the true one-way traveltimes within a given tolerance. When starting with different models or changing optimization parameters, different final models are obtained. All final models explain the input data within the predefined tolerance. Thus, rather than having a single final model, we can obtain several models within the same desired misfit. These models have associated error bars on velocities and depths. We also can answer the question about the amount of velocity and depth information we can get from only

seismic data (without interpreting structures or without a priori knowledge). This is very important in ranking prospects before drilling in areas with no hard velocity-data control.

The basics of this statistical analysis are presented in Figure 2. From a set of initial conditions, we obtain a set of estimated velocity-depth models. Statistical analysis of this set yields six important elements: mean-velocity model, standard deviations of the set of velocity models, mean depths and lateral location of the focal points and standard deviations of the depth, and lateral location of the focal points. Analysis of the set of final models results in four displays: mean-velocity model, velocity standard deviation, mean location of the focal points, and standard deviation of focal points in depth and lateral location.

The optimization involved in the tomographic process is the first characteristic of this approach that enables us to build the space of possible solutions. The performance of a gradient-based method depends strongly on initial values. Therefore, two initial models progress toward two final models. Several optimization runs, each with a different starting point, can lead to different minima, which explain the input data equally well. Although this can be seen as a disadvantage when looking for the global minimum, all final results corresponding to local minima should not be neglected if they explain the data within a reasonable misfit. In our analysis, we do not take possible errors in the input data explicitly into account. To accommodate the effect of errors in the input data, we have chosen a large enough reasonable misfit. In all of our examples, the chosen threshold was 4 ms.

Another item of our approach is data-driven parameterization. This can be used to our advantage when obtaining the space of possible solutions. At each step, model parameterization is based on resolution values of parameters computed in the inversion. Thus, at each step, different grids determine different raypaths and traveltimes. So the initial choice of gridding influences not only the final estimated model but each new data-driven regridding has an impact on the final result. The inversion of new traveltimes leads to a different model, which determines the new regridding. This data-driven model parameterization is the main cause for the existence of local minima. Therefore, the parameterization approach is beneficial because it is data driven and does not need decisions from the user. This approach provides more means of obtaining various estimations of the true model.

We illustrate this statistical analysis on synthetic and field data. For the synthetic data, we chose a model with low- and high-velocity anomalies. For the field data, we used a data set acquired in the Middle East that contains a shallow, high-velocity layer.

The subsurface is governed by geologic laws. Hence, the space of possible subsurface models is restricted as well. Although there are many ways we can arrange layers in the subsurface, some of them disregard geologic constraints. Therefore, the space of models should be confined by geologic rules. For a thorough statistical analysis, the set of input models should span the entire space of models. In our analysis, this is unrealistic because of the enormous computation effort implied. Additionally, complex initial models often lead to nonconverging solutions. Therefore, we start with a wide enough set of initial models containing only homogeneous models and vertical gradients. We include reasonable high- and low-velocity values, letting the data dictate where velocity anomalies exist. We consider this to be the best approach for performing a reliable statistical analysis.

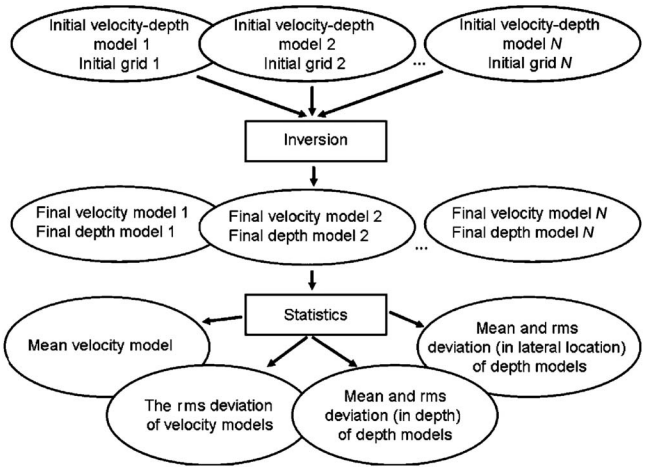

Figure 2. Flowchart describing the statistical analysis for the CFP-based tomographic inversion.

SYNTHETIC EXAMPLE

Our synthetic example is based on a turbidite model (Cox, 2004). It contains a salt dome, fault structures beneath the dome, lateral and vertical velocity gradients within the layers, and a turbidite velocity structure with low velocities (see Figure 3). Representations of these complexities indicate the quality of estimated models.

We first demonstrate our approach to tomographic inversion using this synthetic model. We estimate a velocity-depth model within a misfit of 4 ms starting from a coarse-grid initial velocity model grading vertically from 1.5 to 3.0 km/s and mispositioned initial focal points (Figure 4a and b). The input data are obtained with the maximum offset of 2000 m for the deepest reflector and the focal-point spacing of 300 m along interfaces.

The final estimated velocity-depth model is shown in Figure 4c and d. The salt dome and low-velocity region are visible, although at low spatial resolution. The final estimated focal points follow the structures quite well. However, the deepest boundary is less straight than the true reflector. This first experiment gives us one estimated velocity-depth model that explains the one-way traveltimes within a certain tolerance (4 ms rms difference).

We want to analyze the space of possible models. For this synthetic example, it is easy to obtain real data with various spacings of

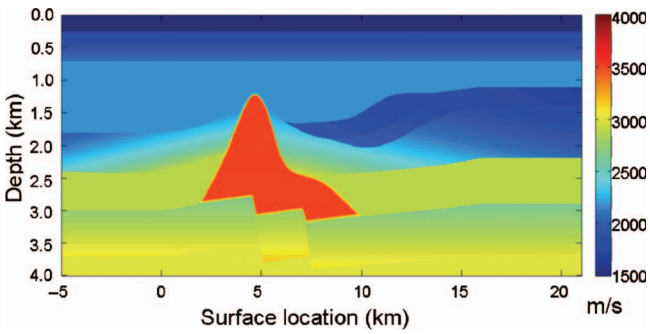

Figure 3. The turbidite velocity model, containing high- and low-velocity anomalies.

focal points or various offsets for traveltime operators. In this way, we analyze the impact of various data sets on the tomographic result. We consider three scenarios: operator spacing of 300 m and maximum offset (for the deepest operators) of 2000 m, operator spacing of 150 m and maximum offset of 2000 m, and operator spacing of 300 m and maximum offset of 3000 m. More scenarios were tested, but these three choices appeared to be the most conclusive. The density of the focal points can be chosen independently of the seismic data. However, the maximum offset of focal operators is coupled directly to the offset in the seismic data. The offset in focal operators corresponds to roughly half the maximum offset in the seismic data.

To compute statistics on estimated models, we need an appropriate number of these models. Therefore, we vary initial velocity models and initial gridding; each such setting corresponds to a final estimated velocity-depth model. The range of initial velocity models contains homogeneous models and vertical velocity gradients. The initial triangulation is based on smaller or bigger grid cells, oriented in various manners; initial focal points are randomly distributed.

Operator spacing 300 m, maximum offset 2000 m

The first experimental data were obtained with a maximum offset of 2000 m and focal-point spacing of 300 m. The final velocity-depth model from Figure 4 is one possible model. Figure 5 shows two other possible velocity-depth models to illustrate how dissimilar estimated models can be, even under the constraint of an rms error in traveltimes below 4 ms, which is met by 52 of 64 estimated models.

Figure 6a and b gives the statistics of the velocity-model ensemble: mean velocity model and standard deviation. Rather than representing one possible model, the mean velocity model in combination with standard deviations represents the ensemble of final models resulting from data with 2000 m offset and 300 m focal points separation.

Figure 7 provides statistics of estimated focal-point locations. The plots give the mean locations of focal points, with the color representing the standard deviation of the vertical and lateral location of focal points. Resolution decreases with an increase in depth, as does the occurrence of artifacts at edges of the model. The contour of the salt dome is quite well defined apart from errors in the location of steeply deeping flanks, whereas the low-velocity region is not well represented, especially its shape.

Corresponding errors in the depths of focal points are generally smaller than 30 m. The lateral locations of focal points also have variations, but they are smaller than their variations in depth, except for flanks of the salt dome that show the biggest errors. The latter information is useful because it provides estimates on the lateral location of features.

Operator spacing 150 m, maximum offset 2000 m

The second scenario corresponds to a denser sampling of focal points and the same maximum offset. We again have various combinations for initial conditions that finalize into 64 estimated models, from which 47 correspond to an rms error of less than 4 ms.

From the resulting set of velocity-depth models, we compute statistics and present the mean and standard deviations. Figure 8 gives statistics of the velocity-model ensemble: mean velocity model and the standard deviation. The statistics of estimated locations are in Figure 9. Plots giving these statistics are not too different from the ones obtained when data corresponding to a lower density of focal points were used, failing to show a substantial improvement. We conclude that in this situation, the 300-m density of focal points is enough to obtain this accuracy and a denser sampling will not translate into smaller errors. This means, for this model, that estimates of focal operators need to be completed for a density of 300 m only.

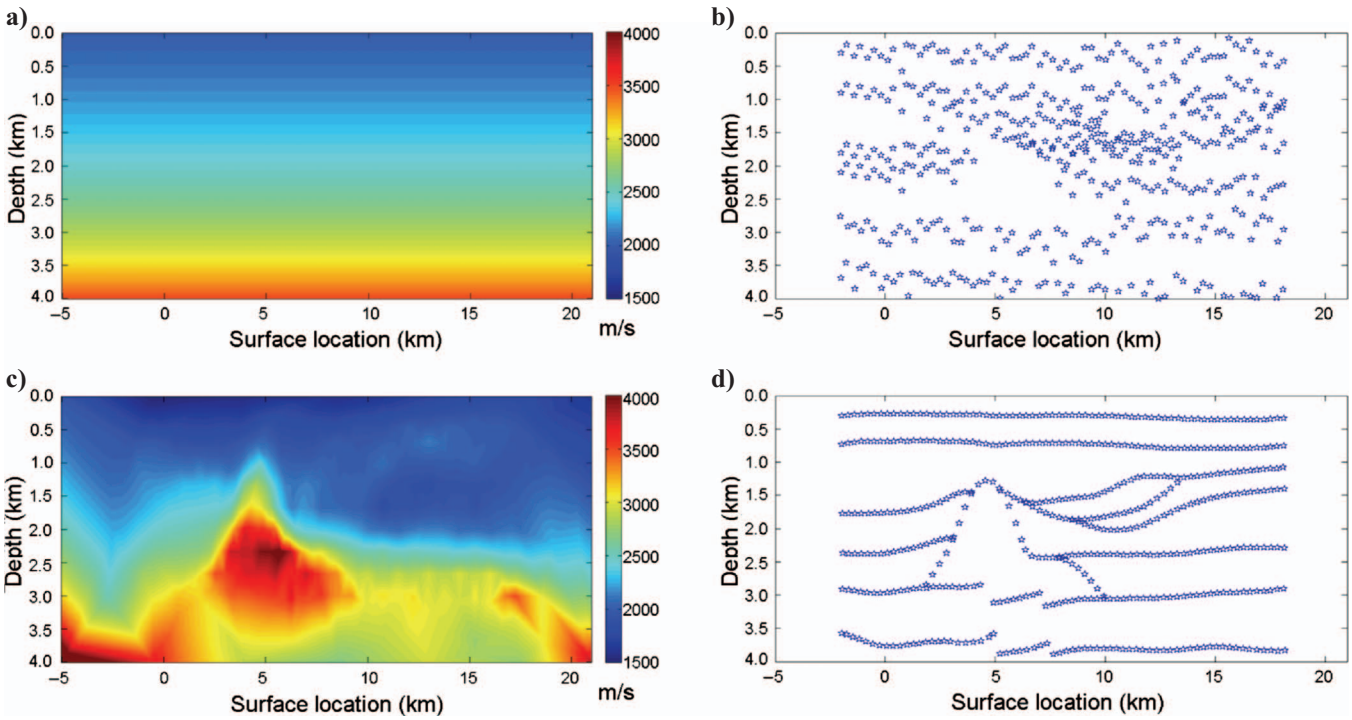

Figure 4. (a)Initial velocity model. (b) Initial focal-point locations. (c) The final estimated model after tomographic inversion. (d) Estimated focal-point locations.

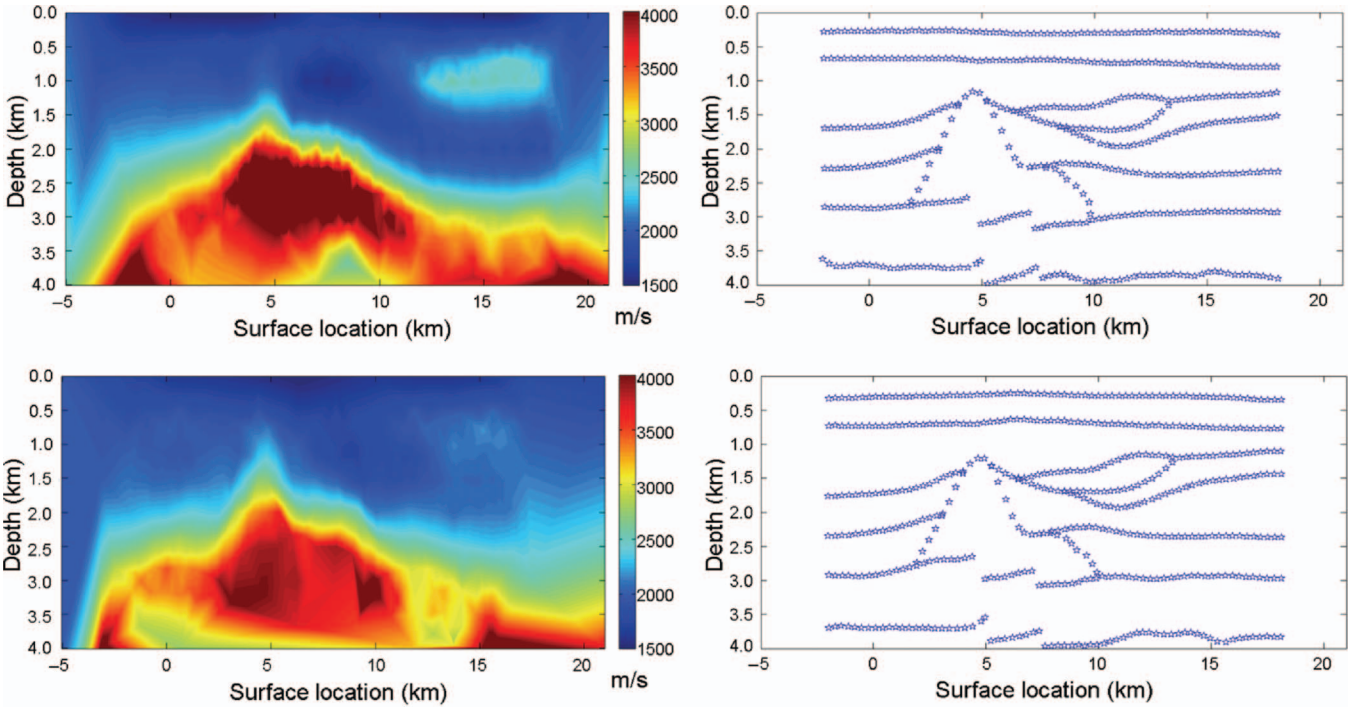

Figure 5. Two examples of estimated velocity-depth models resulting from the tomographic inversion with different initial settings.

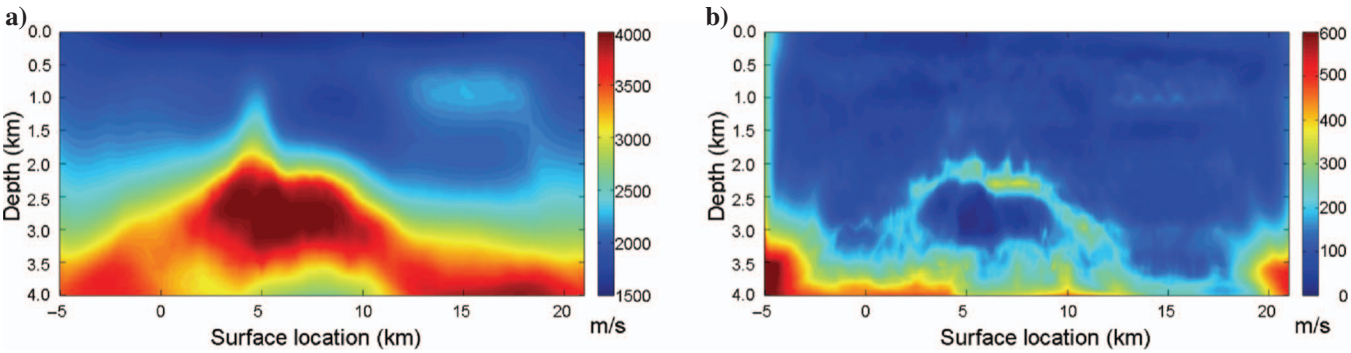

Figure 6. Statistics for estimated velocity models in scenario 1 (maximum offset = 2 km, focal-point spacing = 300 m): (a) mean velocity model; (b) standard deviation of velocity models.

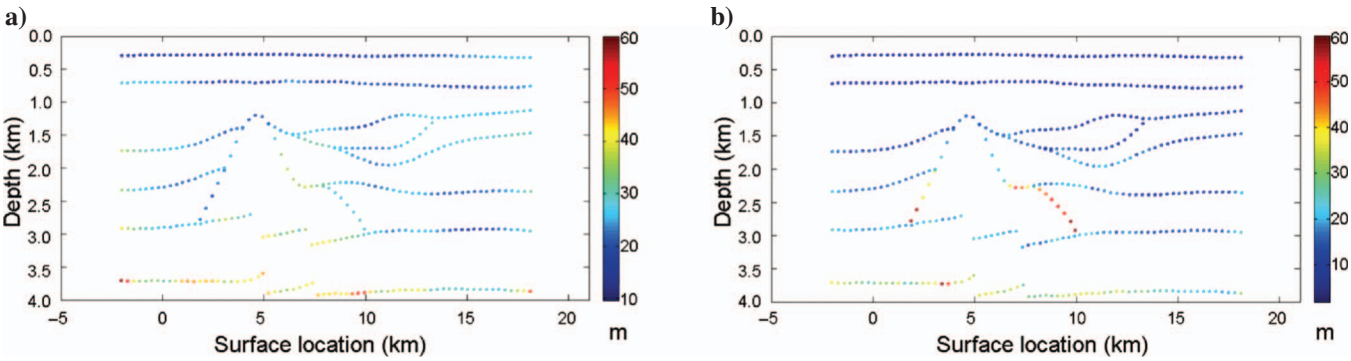

Figure 7. Statistics for focal-point locations in scenario 1 (maximum offset = 2 km, focal-point spacing = 300 m). Color represents standard deviation of a focal-point location: (a) vertical; (b) lateral.

Operator spacing 300 m, maximum offset 3000 m

The third scenario corresponds to the reference density of focal points (one every 300 m) and a larger maximum offset of 3000 m. This mimics the acquisition with 6-km-long instead of 4-km-long cables.

Statistics of the 63 estimated velocity models that met the chosen traveltime misfit are presented in Figure 10. Figure 11 presents statistics of the estimated locations. We notice a much better delineation of the salt dome and region of low velocity. Even depths of estimated focal points have smaller errors, mostly below 30 m. We can conclude that data obtained from wider operators improved the accuracy of estimated velocity models and focal-point depths. This is very important for the acquisition design phase of seismic surveys. This analysis can be completed before seismic data acquisition with an estimate of the velocity-depth model (Al-Ali, 2007).

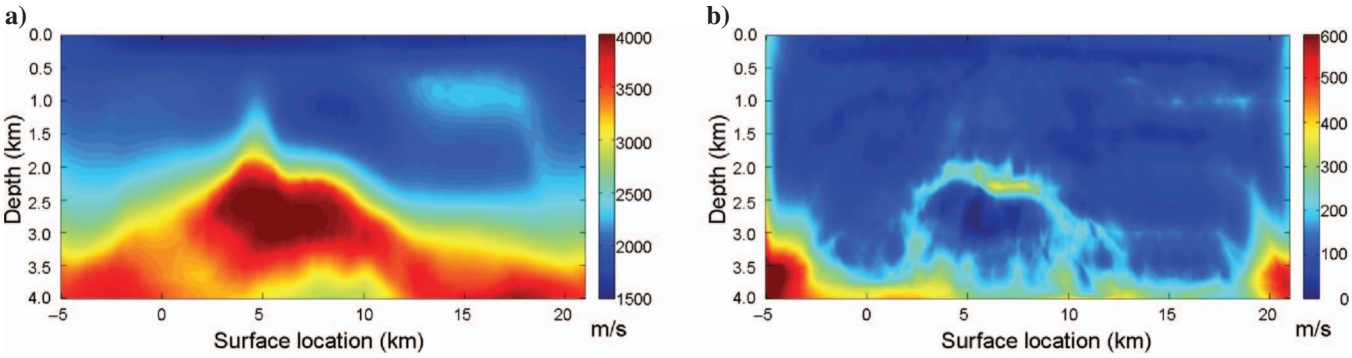

Figure 8. Statistics for estimated velocity models in scenario 2 (maximum offset = 2 km, focal point spacing = 150 m): (a) mean velocity model; (b) standard deviation of the velocity models.

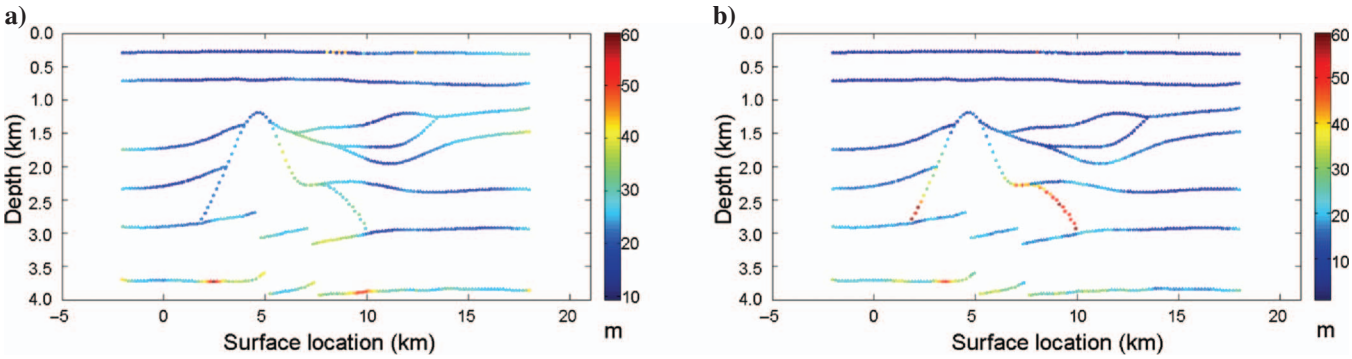

Figure 9. Statistics for focal-point locations in scenario 2 (maximum offset = 2 km, focal points spacing = 150 m). Color represents standard deviation of a focal-point location: (a) vertical; (b) lateral.

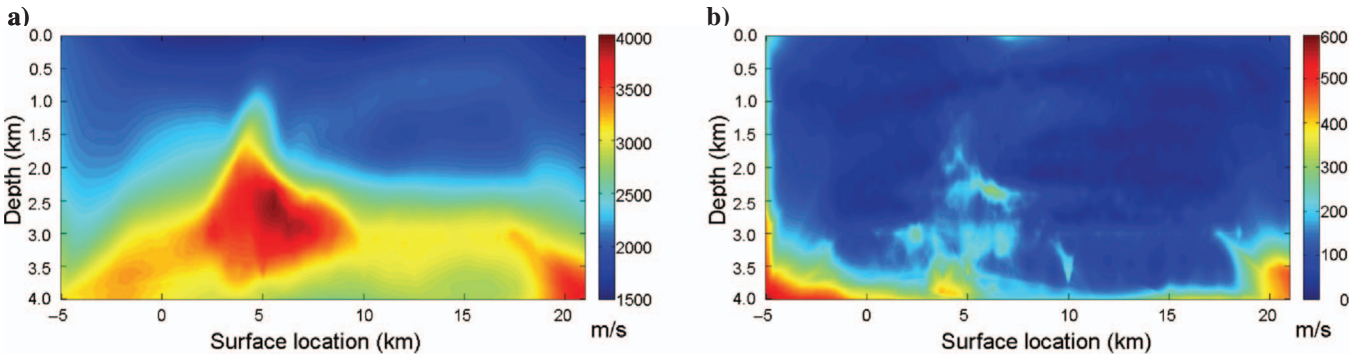

Figure 10. Statistics for estimated velocity models in scenario 3 (maximum offset = 3 km, focal-point spacing = 300 m): (a) mean velocity model; (b) standard deviation of velocity models.

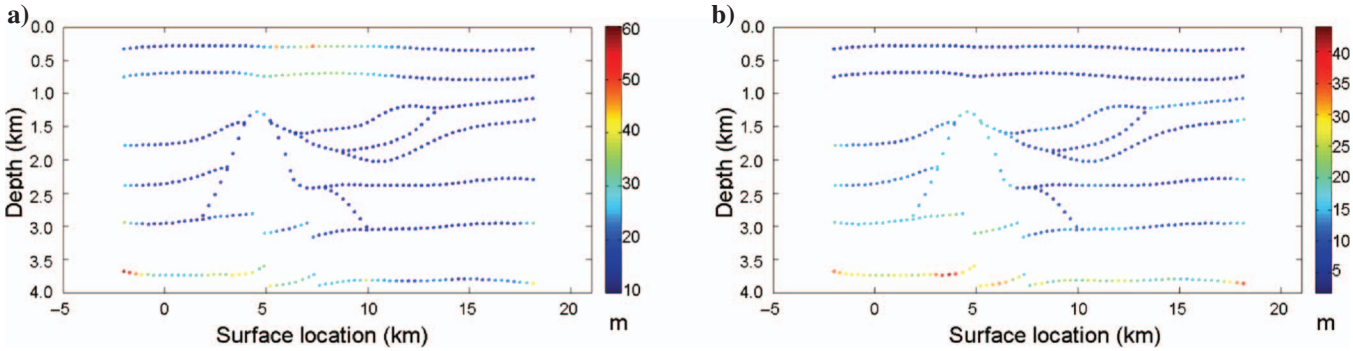

Figure 11. Statistics for focal-point locations in scenario 3 (maximum offset = 3 km, focal-point spacing = 300 m). Color represents standard deviation of a focal-point location: (a) vertical; (b) lateral.

FIELD DATA EXAMPLE

We demonstrate the CFP approach to prestack migration by presenting a complete work flow. First, the one-way-time focusing operators are estimated from two-way-time seismic data. Using these operators, the velocity-depth model is obtained via tomographic inversion of focusing operators. Finally, prestack depth migration (PSDM) is performed using the estimated velocity model. Furthermore, we compare the final velocity model with the one obtained using a commercial two-way traveltime reflection-tomography package. The comparison proves the superiority of our approach based on the data-driven parameterization and global inversion, as opposed to the layer-stripping approach and restricted-layered parameterization inherent in the commercial-tomographic package approach.

The data used consist of a 2D line extracted from a 3D data set acquired in Saudi Arabia. Figure 12 presents a stack resulting from conventional NMO velocity analysis, showing a layer-cake subsurface model. Nine reflectors were chosen to estimate corresponding one-way-time operators, indicated by arrows. Static shifts were applied to account for surface elevation.

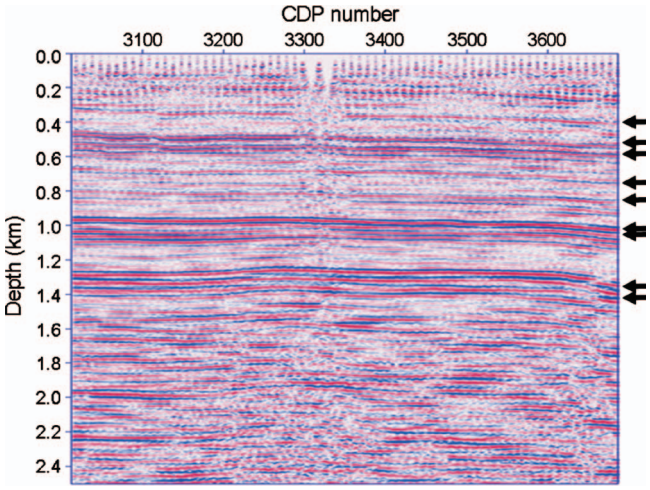

Figure 12. Stacked section of the field data. Arrows indicate the nine reflectors used in velocity estimation.

Velocity estimation using one-way traveltime tomography

The first step of transforming two-way-time data into one-way-time data is based on Fermat's principle (Al-Ali et al., 2007). This principle states that the wave path between two points is a path of stationary time. The one-way operators, in this case, were inverted simultaneously per boundary from tracked two-way reflection times using a preconditioned conjugate gradient method. The inverted operators were validated using differential-time-shift (DTS) gathers. In some locations, these operators were updated further using residual times of DTS gathers (Bolte and Verschuur, 1998). We use 103 operators per reflector, which is a focal-point spacing of approximately 120 m, and only the reliable offsets for operators, varying from 400 m for the shallow one to 1100 m for deeper ones. (For more details on this part of the experiment, see Al-Ali and Verschuur, 2006.)

Estimated focusing operators (see Figure 13) form the input for the tomographic inversion. The velocity-depth model obtained with focusing-operator tomography is presented in Figure 14a and it corresponds to a final rms error of 3.2 ms. The estimated nine reflectors also are present in the plot; the velocity varies between reflectors within the limitations of a smooth model. We expect further improvement by including extra boundaries below the deepest one.

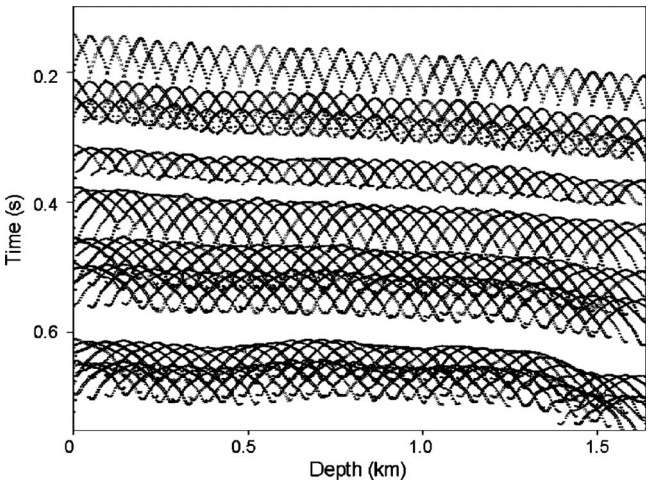

Figure 13. Estimated focusing operators for the nine reflectors in Figure 12. These operators form the input of one-way traveltime tomography.

This will provide better illumination of the bottom of the model and therefore an improved estimate of depths and velocities, especially concerning the low-velocity region below the seventh reflector.

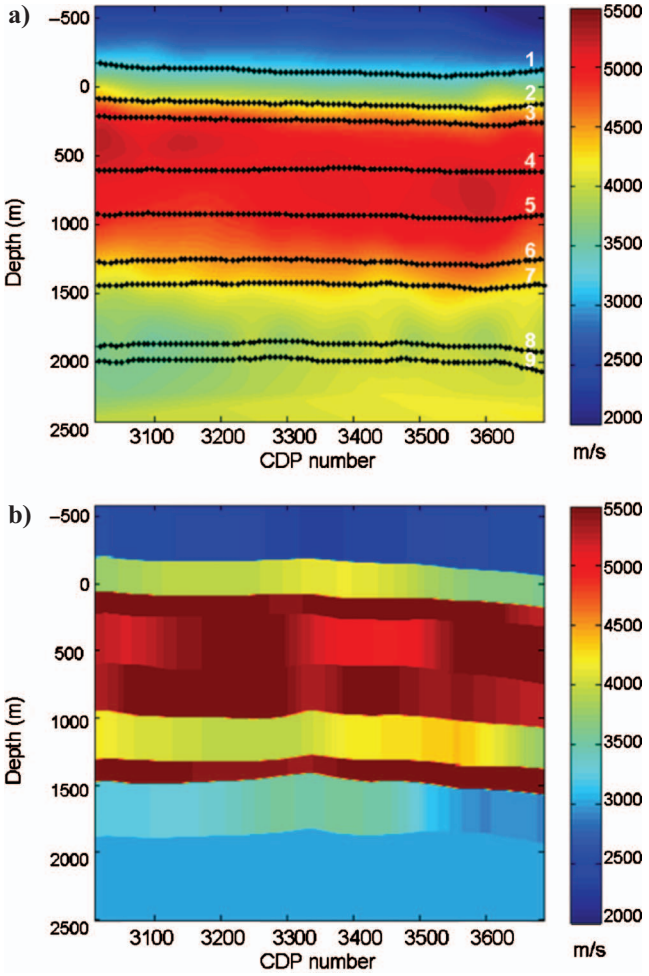

Figure 14. Velocity model for the field data estimated with (a) one-way common-focal-point traveltime tomography and (b) a commercial two-way traveltime tomography package.

Velocity estimation using two-way traveltime tomography

We compare a result obtained with the tomographic inversion of focusing operators (Figure 14a) with the result of a two-way traveltime reflection-tomography software package (Figure 14b). The latter result clearly shows the disadvantages of a layer-stripping approach. Moreover, there were some problems inverting the third reflector, which translated into higher and poorly concentrated traveltime residuals, shown in Figure 15b. The error distribution obtained with the one-way traveltime tomography is presented in Figure 15a. Errors are well concentrated and mostly fall between -5 and 5 ms.

Validation of estimated models via PSDM

Next, a PSDM was applied using both models. The two plots in Figure 16 present the resulting depth images. There are differences in both images, but it is difficult to judge the quality of each. However, CIGs generated from both models (Figure 17) show flatter events corresponding to the model estimated with one-way traveltime tomography.

We conclude that in terms of residuals and the quality of CIGs, the CFP approach to tomographic inversion gave better velocity-estimation results. The method is superior because of the data-driven parameterization (versus restricted-layer parameterization) and the global-inversion approach (all boundaries together versus the layer-stripping approach).

Evaluating uncertainty from an ensemble of models

We performed the same statistical analysis done on the synthetic data for the field data. To obtain the space of models, we used different initial velocity models (with various vertical gradients or homogeneous values) with variable initial gridding. We also used various initial-focal-point distribution, either concentrated mostly around initial boundaries or spread randomly. We ran the tomographic inversion for each such combination of initial settings. Of 96 solutions, 69 met the desired criterion of a final rms error of less than 4 ms within a given maximum number of updates.

Estimated models present variations in velocity values and depths. The reasonable misfit of less than 4 ms allows for a large space of models. Figure 18 presents an idea of the amount of varia-

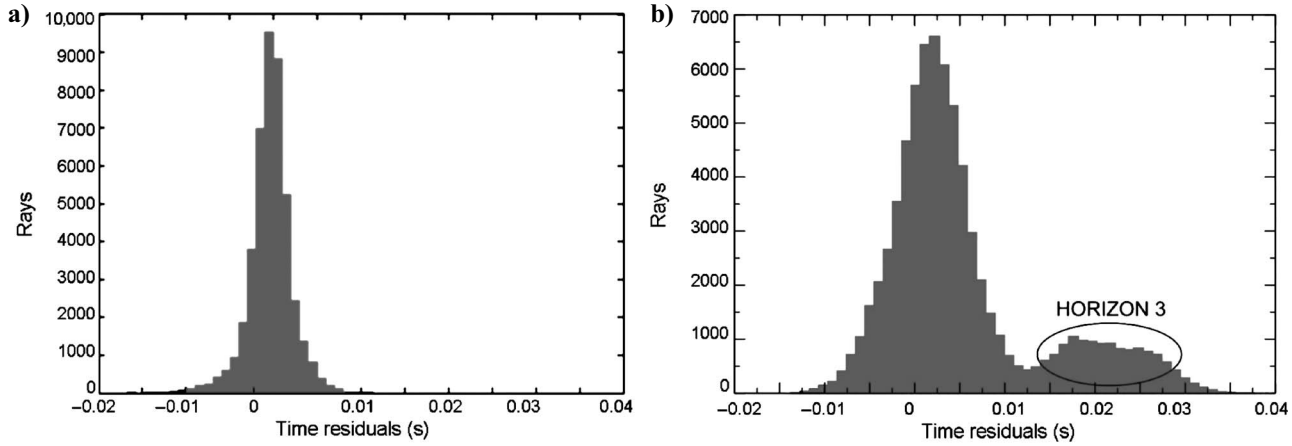

Figure 15. Histogram of time residuals after (a) one-way CFP traveltime tomography and (b) a commercial two-way traveltime tomography package.

tion possible. These variations might have a large impact on deduced properties, such as pressure-prediction values. Figure 19 gives statistics of the velocity-model ensemble — mean velocity model and the standard deviation. As mentioned, when analyzing the synthetic example, the mean model is not a possible model. However, along with the obtained standard deviation, it can give an indication about the space of models and obtained variations. Values are as much as 600 m/s for the standard deviation. However, biggest variations are at the edges and bottom of models (note the high-velocity layer at the bottom of the model). These areas contain a limited number of raypaths, which results in fewer grid points and translates into a less-satisfactory estimate of those regions. In the shallow part of the model, the maximum variation is 200 m/s; in deep parts, it is smaller than 430 m/s. Generally, the resolution decreases with depth following the decrease in the angle coverage caused by the limited surface-recording geometry.

Statistics of estimated depths are given in Figure 20a. The first plot gives the mean locations of focal points, with color representing the standard deviation of the depths of focal points. The same decrease in resolution is observed as we go deeper. We reemphasize the need for a new boundary, below the last one, to better illuminate the bottom of the model. However, the accuracy in estimating depths is quite good, with values above 50 m only in expected regions of less information.

Another important attribute is the variation in layer thickness. Such data can be used to assess the uncertainty of reservoir volume. Figure 20b gives the coefficient of variation (the ratio between the standard deviation and the mean) reported as a percentage, or what is called relative standard deviation. This result can be interpreted as the accuracy of the thickness of estimated layers. Despite large variations in the velocity depth, the thickness of layers is quite robust (variations smaller than 10 m), except for the last one.

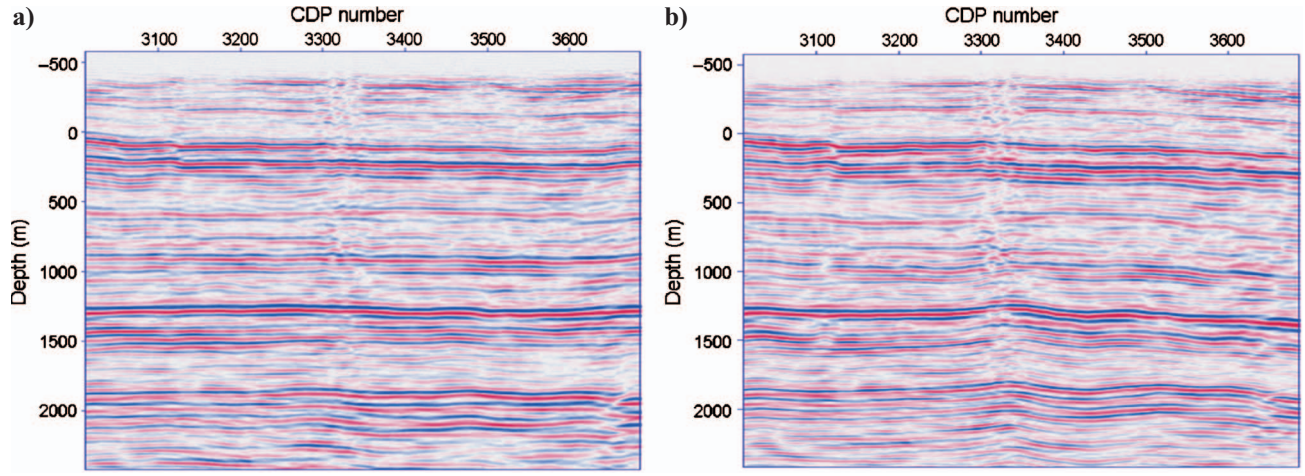

Figure 16. PSDM of the field data using the velocity model estimated with (a) one-way CFP traveltime tomography and (b) a commercial two-way traveltime tomography package.

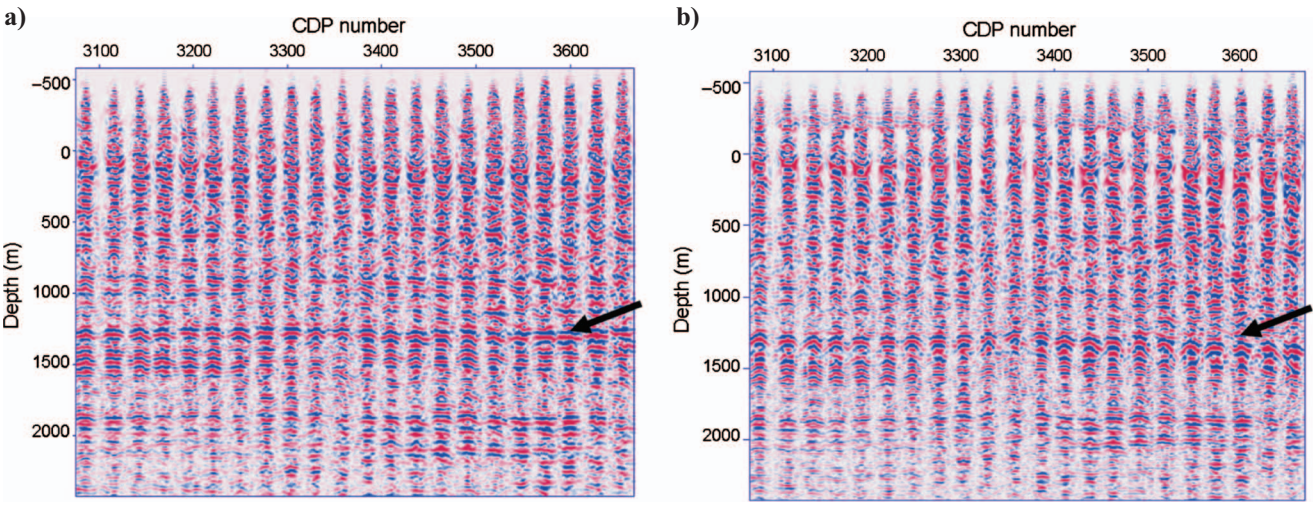

Figure 17. CIGs for the field data after migration using velocity models estimated with (a) one-way CFP traveltime tomography and (b) a commercial two-way traveltime tomography package. Note the improved features of events in (a) around 1300 m depth.

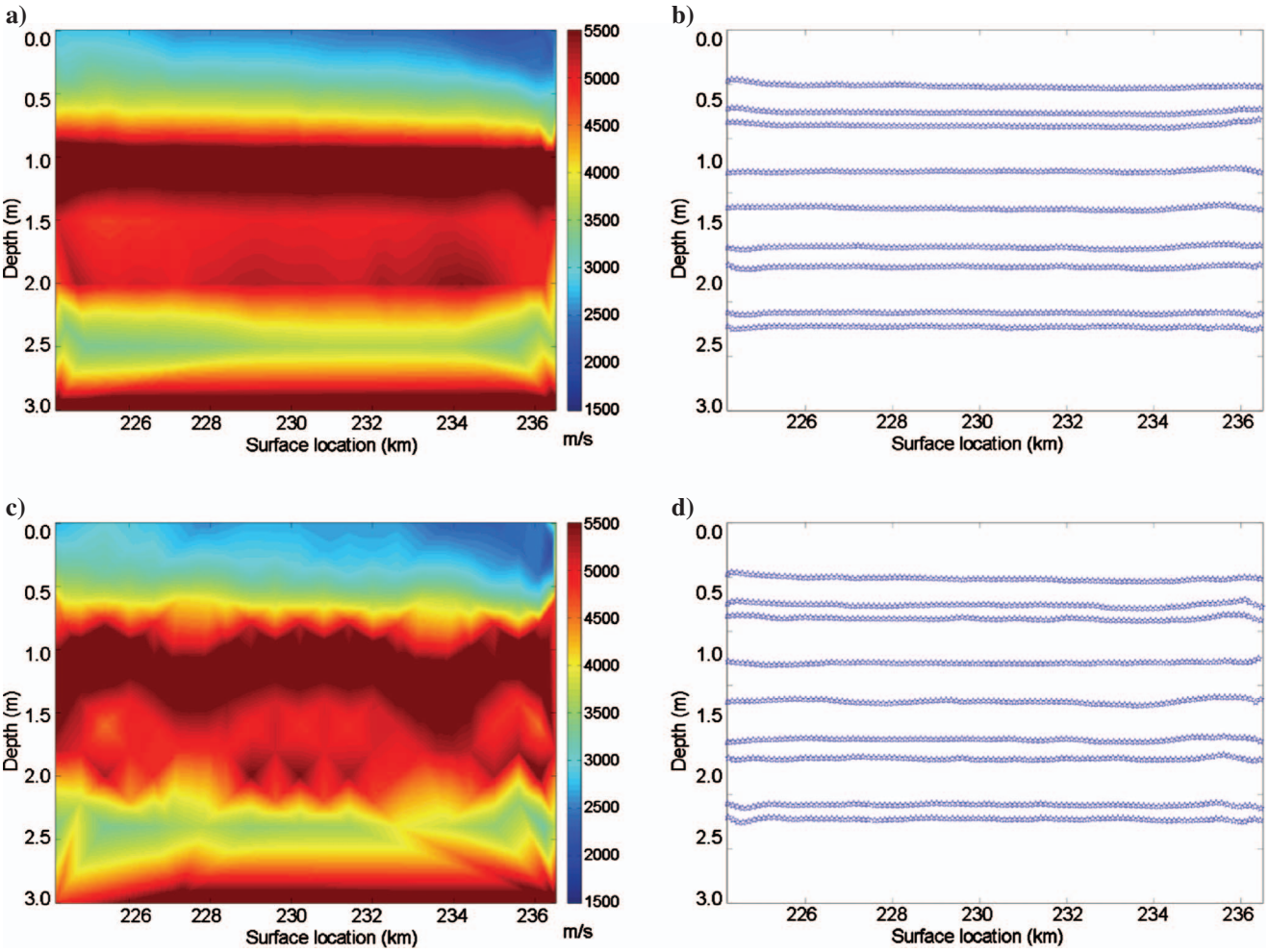

Figure 18. Two examples of estimated velocity-depth models that fit input traveltimes within 4 ms rms. Note large differences with possible large impact on deduced properties, such as pressure-prediction values.

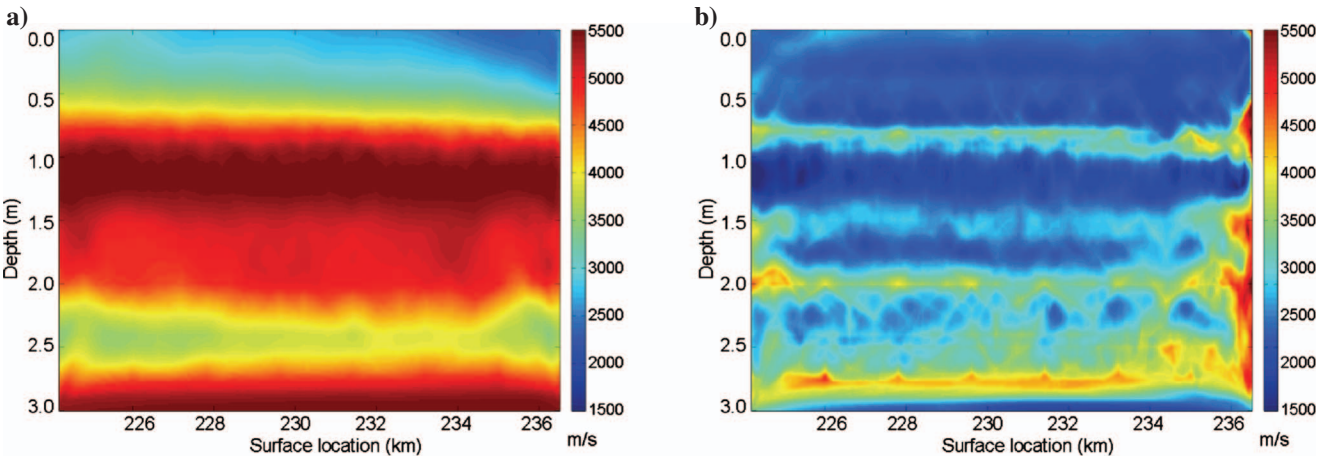

Figure 19. Statistics for velocity models: (a) mean velocity model; (b) standard deviation of velocity models.

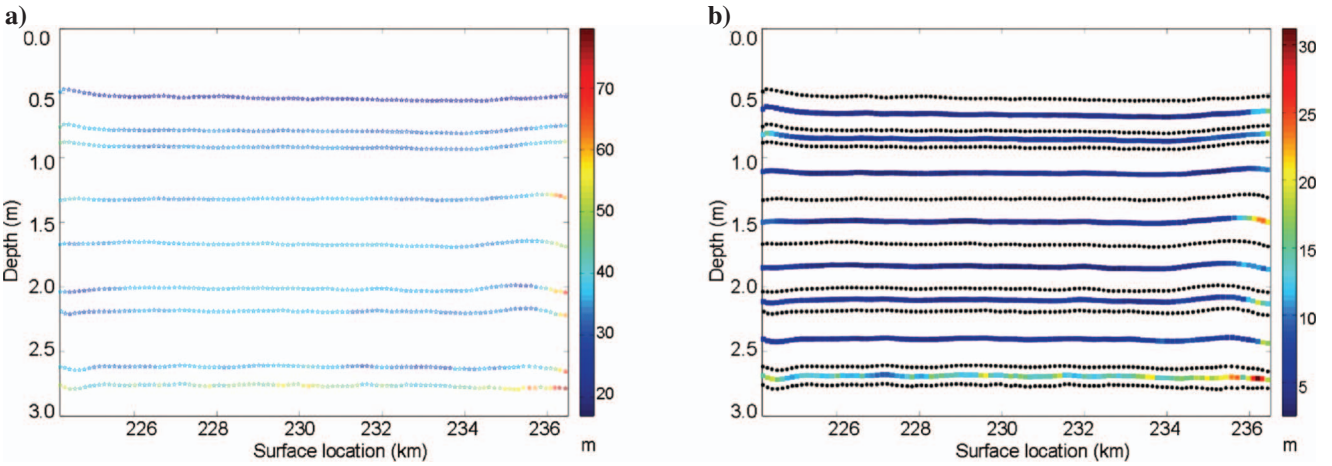

Figure 20. Statistics for focal-point locations: (a) mean and standard deviation of depth; (b) accuracy of thickness. Color represents (a) standard deviation of the depth of the focal point; (b) standard deviation of layer thickness.

CONCLUSIONS

Estimating velocity models via tomographic inversion is a very complex problem. Ideally, such an inversion should consist of two parts: a model estimate followed by an assessment of solution accuracy. Often, only the first part is completed. We have concentrated on the second part, considered to be at least equally important as the first one.

We performed several tomographic inversions for focusing operators modeled for a synthetic data set, and estimated from field data in the Middle East by varying initial settings to obtain an ensemble of possible models. All obtained models fit the input data within the same reasonable misfit. Estimates of the error bars associated with solutions are presented by performing a statistical analysis of all obtained models. The mean velocity and depth models, along with the standard deviations, can be evaluated to establish the accuracy of estimates. Leaving aside edge effects, we conclude that our estimates have reasonably good accuracy. One of the most important results shows the coefficient of variation in the thickness of different velocity layers for the field data. Again, with the exception of the edges and the thickness associated with the last layer, we obtain values of about 5%, proving that a small fraction of models varies significantly from the mean.

All obtained results can help identify areas in which it is necessary to add extra information. This might provide important feedback for acquisition-geometry design. If the analysis shows uncertainty values larger than acceptable, new data are needed to decrease this ambiguity. This could be either reacquiring seismic data with more offsets or including hard information, such as well logs.

ACKNOWLEDGMENTS

We acknowledge Saudi Aramco for providing the field data used for this study. We thank Emad Al-Janoubi for his assistance in estimating the velocity model from the tracked two-way reflection times using a commercial reflection-tomography software package.

REFERENCES

Al-Ali, M. N., 2007, Land seismic data acquisition and preprocessing: An operator solution to the near-surface problem: Ph.D. thesis, Delft University of Technology.

Al-Ali, M. N., G. Blacquière, and D. J. Verschuur, 2007, From tracked two-way reflection times to redatuming: An operator approach: 77th Annual International Meeting, SEG, Expanded Abstracts, 2600–2603.

Al-Ali, M. N., and D. J. Verschuur, 2006, An integrated method for resolving the seismic complex near-surface problem: Geophysical Prospecting, **54**, 739–750.

Al-Yahya, K., 1989, Velocity analysis by iterative profile migration: Geophysics, **54**, 718–729.

Berkhout, A. J., 1997a, Pushing the limits of seismic imaging—Part I: Prestack migration in terms of double dynamic focusing: Geophysics, **62**, 937–953.

———, 1997b, Pushing the limits of seismic imaging—Part II: Integration of prestack migration, velocity estimation, and AVO analysis: Geophysics, **62**, 954–969.

Bishop, T. N., K. P. Bube, R. T. Cutler, R. T. Langan, P. L. Love, J. R. Resnick, R. T. Shuey, D. A. Spindler, and H. W. Wyld, 1985, Tomographic determination of velocity and depth in laterally varying media: Geophysics, **50**, 903–923.

Böhm, G., and A. L. Vesnaver, 1999, In quest of the grid: Geophysics, **64**, 1116–1125.

Bolte, J. F. B., and D. J. Verschuur, 1998, Aspects of focusing operator updating: 68th Annual International Meeting, SEG, Expanded Abstracts, 722–725.

Cox, B., 2004, Tomographic inversion of focusing operators: Ph.D. thesis, Delft University of Technology.

Cox, B. E., and D. J. Verschuur, 2001, Tomographic inversion of focusing operators: 63rd International Conference and Exhibition, EAGE, Extended Abstracts, session M-35.

Hegge, R. F., 2000, Seismic macromodel estimation by inversion of focusing operators: Ph.D. thesis, Delft University of Technology.

Kosloff, D., Z. Koren, E. Machet, and Y. Falkovitz, 1996, Velocity and interface depth determination by tomography of depth migation gathers: Geophysics, **61**, 1511–1523.

Paige, C., and M. Saunders, 1982, LSQR: An algorithm for sparse linear equations and sparse least squares: ACM Transactions on Mathematical Software, **8**, 43–71.

Rietveld, W. E. A., 1995, Controlled illumination in prestack seismic migration: Ph.D. thesis, Delft University of Technology.

Sambridge, M., M. Braun, and H. McQueen, 1995, Geophysical parameterization and interpolation of irregular data using natural neighbours: Geophysical Journal International, **122**, 837–857.

Stork, C., 1992, Reflection tomography in the postmigrated domain: Geophysics, **57**, 680–692.

Thorbecke, J. W., 1997, Common focus point technology: Ph.D. thesis, Delft University of Technology.

van der Made, P. M., 1988, Determination of macro subsurface models by generalized inversion: Ph.D. thesis, Delft University of Technology.

Vesnaver, A. L., G. Böhm, and O. G. S. Italy, 1995, Tomography of a tomographic grid: 65th Annual International Meeting, SEG, Expanded Abstracts, 1047–1050.